

A Simplified Model for Predicting the Power Delay Profile Characteristics of an Indoor Radio Propagation Channel

**Christopher L. Holloway
Michael G. Cotton
Paul McKenna**



**U.S. DEPARTMENT OF COMMERCE
William M. Daley, Secretary**

Larry Irving, Assistant Secretary
for Communications and Information

August 1998

CONTENTS

| | Page |
|---|------|
| FIGURES | v |
| ABSTRACT | 1 |
| 1. INTRODUCTION | 1 |
| 2. BACKGROUND..... | 4 |
| 3. INDOOR POWER DELAY PROFILE MODEL..... | 5 |
| 3.1 Characteristic Time t_c of a Room | 7 |
| 3.2 Reflected Power Levels | 7 |
| 3.3 Direct Ray | 9 |
| 3.4 Power Delay Profile..... | 10 |
| 3.5 Room Consisting of Different Reflecting Surfaces..... | 10 |
| 4. GEOMETRY AND MATERIAL PROPERTIES VARIATIONS..... | 11 |
| 5. WIDEBAND SYSTEMS | 13 |
| 6. VALIDATION OF THE MODEL..... | 15 |
| 7. DISCUSSION AND CONCLUSION..... | 19 |
| 8. ACKNOWLEDGMENTS..... | 21 |
| 9. REFERENCES | 22 |

FIGURES

| | Page |
|---|------|
| Figure 1. Propagation-link diagram..... | 2 |
| Figure 2. Output waveform for a two-ray multipath channel..... | 3 |
| Figure 3. Typical field level distribution inside a room..... | 6 |
| Figure 4. Probabilities of travel times of rays making n bounces..... | 8 |
| Figure 5. Normalized power delay profile (PDP) model..... | 10 |
| Figure 6. Variations of the PDP for different size rooms | 12 |
| Figure 7. Variations of the PDP for different types of wall materials | 12 |
| Figure 8. Variations of the PDP for different ceiling materials..... | 13 |
| Figure 9. Variations of the PDP for a room with different materials in one wall..... | 14 |
| Figure 10. Variations of γ for a room with different types of reflecting surfaces..... | 14 |
| Figure 11. Comparison of the IPDP model to the FDTD simulation..... | 16 |
| Figure 12. Comparison of the IPDP model to the FDTD simulation..... | 17 |
| Figure 13. Comparison of the IPDP model to measured data for a small office | 18 |
| Figure 14. Comparison of the IPDP model to measured data for a laboratory | 19 |
| Figure 15. Comparison to measured data obtained by averaging several locations..... | 20 |
| Figure 16. Comparison to measured data obtained by averaging several locations..... | 20 |

A SIMPLIFIED MODEL FOR PREDICTING THE POWER DELAY PROFILE CHARACTERISTICS OF AN INDOOR RADIO PROPAGATION CHANNEL

Christopher L. Holloway, Michael G. Cotton, and Paul McKenna*

Multipath channels in indoor wireless communication systems exhibit a characteristic power delay profile, which can be a detriment to system performance. In this paper, we present a simplified model for calculating the decay rate of the power delay profile for propagation within rooms. This simplified model provides a time-efficient means of predicting system performance. Predictions of this indoor power delay profile (IPDP) model are compared to results obtained from a finite-difference time-domain (FDTD) model. Additionally, comparisons of the IPDP model to measured data are presented. The rms delay spread is the second central moment of the power delay profile of a propagation channel and is a measure of the communication link degradation due to multipath. We also show results of the estimated rms delay spread from this model and show comparisons to the measured data. This IPDP model can be used to investigate the effects of variable room size and properties of the surfaces (or walls) on the decay characteristics of the power delay profile.

Key words: multipath; power delay profile; channel modeling; delay spread; impulse response; finite-difference time-domain modeling

1. INTRODUCTION

In designing wireless telecommunication systems, it is crucial to control the intersymbol interference (ISI) and more importantly the bit error rate (BER). The ISI is directly related to the multipath phenomena resulting from objects (such as walls, furniture, and people) in the propagation path between the transmitter and receiver. The delay spread of the radio propagation channel is a measure of the multipath effects which are a detriment to system performance [1]-[10].

The channel effects of a transmitted signal can be interpreted by the propagation-link diagram shown in Figure 1. In this figure, $s(t)$ is a symbol waveform of the transmitted signal before propagating through the indoor channel, $h(t)$ is the impulse response of the indoor channel, and $o(t)$ is the symbol waveform after propagating through the indoor channel. The waveform at the output of the channel $o(t)$ is the convolution of $s(t)$ and $h(t)$ in the time-domain or the multiplication of the respective quantities in the frequency-domain

$$O(\omega) = S(\omega)H(\omega), \quad (1)$$

*The authors are with the Institute for Telecommunication Sciences, National Telecommunications and Information Administration, U.S. Department of Commerce, Boulder Laboratories, Boulder, CO, 80303.

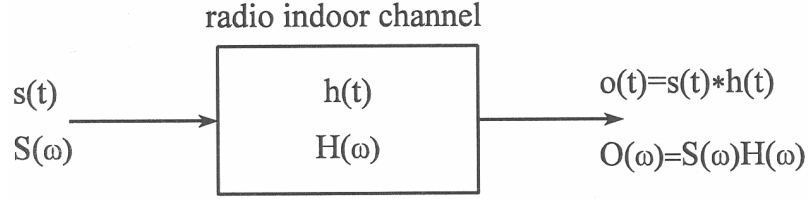


Figure 1. Propagation-link diagram.

where $O(\omega)$, $S(\omega)$, and $H(\omega)$ are the Fourier transforms of $o(t)$, $s(t)$, and $h(t)$, respectively. For a frequency flat-fading channel (i.e., $H(\omega) = 1$) no distortion in $o(t)$ will occur and $o(t) \equiv s(t)$. The effects of multipath are best illustrated with a simple two-ray multipath channel. The normalized impulse response that corresponds to a direct ray and one reflected ray, is approximated by

$$h(t) \approx \delta(t) + R \exp^{-j\omega\tau_1} \delta(t - \tau_1). \quad (2)$$

For simplicity, the reflection coefficient R of the scatterer is set to unity. The delay of the reflected ray is given by

$$\tau_1 = \Delta r / c,$$

where Δr is the difference in the path length between the direct and reflected rays and c is the speed of propagation of electromagnetic waves. For this two-ray channel model, the magnitude of $H(\omega)$ is

$$|H(\omega)| \propto |\cos(\omega\tau_1 / 2)|. \quad (3)$$

The nulls of $|H(\omega)|$ occur at frequencies of $\omega_n = \frac{\pi}{\tau_1} (2n - 1)$. As τ_1 increases, which occurs for increasing Δr , the first null of $|H(\omega)|$ approaches $\omega = 0$.

Assuming that the transmitted symbol waveform is a square wave of pulsewidth T , the Fourier transform of $s(t)$ is a sinc function

$$S(\omega) \propto \frac{\sin(\omega T / 2)}{\omega T / 2}. \quad (4)$$

Utilizing the channel frequency-domain response given in equation (3), the waveform at the output of the channel can be obtained by equation (1). The output waveform $O(\omega)$ was calculated for various values of τ_1/T for this two-ray channel and is shown in Figure 2. The input signal $S(\omega)$ is also displayed in this figure. The channel acts as a frequency filter on the symbol waveform, and as long as the first null of the frequency-domain channel response is much greater than $\omega = \frac{2\pi}{T}$, there will be little distortion of the symbol

waveform at the output of the channel. When τ_1 is comparable to T , distortion in the output waveform will occur. Thus, for $\tau_1 \ll T$, little degradation of the output waveform will occur, and $O(\omega) \approx S(\omega)$. In Figure 2, it is seen that the results for $O(\omega)$ with $\tau_1 = .1T$ lays on top of $S(\omega)$. Whereas, for $\tau_1 \gg T$, severe degradation in the waveform is shown. These results can be interpreted in the following manner: for a well-defined or constant multipath delay τ_1 ,

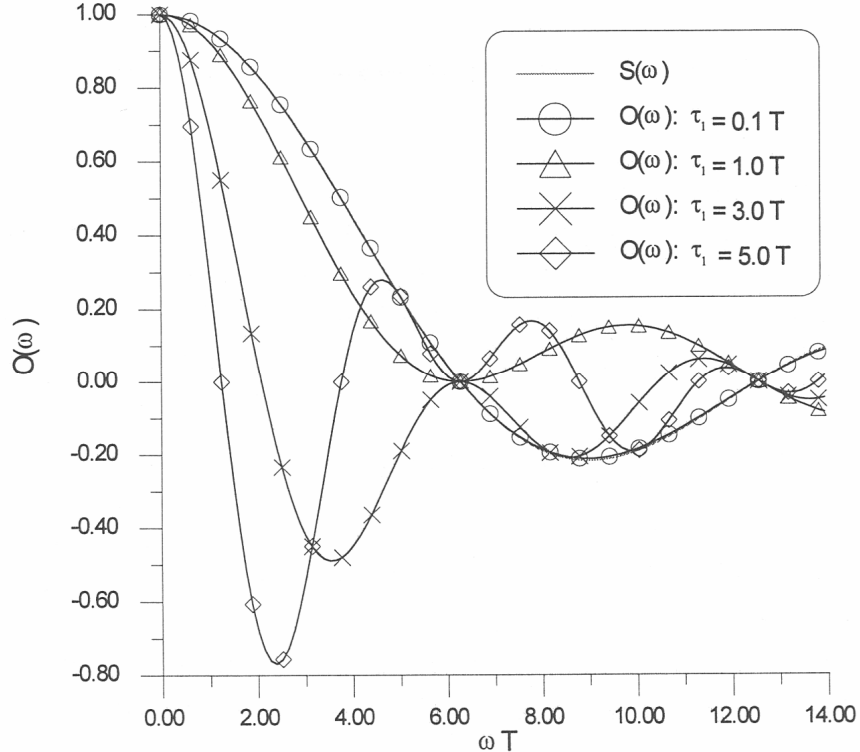


Figure 2. Output waveform for a two-ray multipath channel.

the pulsewidth T of the transmitted waveform may need to be increased in order to reduce distortion. An increase in T essentially means a decrease in the data rate.

While a simple two-ray impulse response model was used to illustrate the effects of multipath, more realistic multiple-ray channels have the same effects [1]-[10]. That is, as long as the multipath delay is small compared to the symbol period T , a signal can propagate through a multipath channel with little distortion. However, the distortion due to a large delay spread (the delay spread is the second central moment of the impulse response of a propagation channel) affects the BER and the feasible data rates. This is illustrated by Chuang [1], where it is shown that the BER in ISI-limited wireless systems is proportional to the square of the ratio of the delay spread to the symbol period. Therefore, in choosing the maximum data rates for a particular system, it is important to know the delay spread for the indoor environment where the system is to be deployed.

While techniques such as equalization [11], [12] and diversity [13]-[15] are often used to mitigate the effects of multipath, it is still important to be able to predict the multipath effects by estimating the impulse response and decay rates in the indoor channel before designing a particular system. There are various techniques available for predicting these multipath effects. Geometric optics (or ray tracing) models [16]-[29], finite-difference time-domain (FDTD) models [30]-[33], and time-domain integral equation models [34] have been used to calculate the impulse response and the power delay profile for indoor channels. While both the FDTD and the ray tracing techniques are accurate, they are time consuming.

Statistical models for indoor radio propagation have also been developed for determining the impulse response [35]-[44]; however, these models are only valid as long as the defining statistics for the channel being modeled are accurate.

In this paper we introduce a simplified model for calculating the power delay profile for indoor wireless radio propagation channels. Parameters in this model are functions of the volume of the room, the surface area of the room, and the amount of energy absorbed into the walls. The predictions from this indoor power delay profile (IPDP) model are compared to numerical results obtained from a FDTD model, as well as to measured data.

2. BACKGROUND

Dating back to the turn of the century, the acoustic community has been estimating the decay rates (or reverberation time) of energy inside acoustic cavities (or rooms) [45]-[55]. Reverberation of a room occurs when multiple wall reflections are present [56]. Under this condition, the field levels in an acoustic cavity are assumed to be uniform, and the gross tendency of the average energy W in the room resembles an exponential decay

$$W(t) = W_o \exp^{(-t/\tau)}. \quad (5)$$

The expression is usually referred to as the Sabine reverberation equation [48], where T is the characteristic decay time and is given by

$$\tau = \frac{4V}{vS\alpha}, \quad (6)$$

where V is the volume of the room, S is the surface area of the walls in the rooms, v is the speed which energy propagates in the room (for acoustic rooms, this is the speed of sound), and α is the acoustic absorption coefficient defined in [57] and [58].

This approach has been used to calculate the characteristic decay times and the Q of the acoustic cavity (defined as $Q = \omega\tau$) for electromagnetic reverberation chambers [59]-[64]. The dissipated energy in the highly conducting walls of these reverberation chambers has been determined by averaging over the individual cavity modes [60] and [63] and by averaging plane wave losses due to reflections over all possible angles of incidence and polarizations [62] and [65]. The latter approach will be utilized in this paper to approximate the power dissipated and reflected by the surfaces (or walls) in rooms.

The above approach for determining the decay time of reverberation rooms, works very well as long as the absorption coefficient α is small. As α approaches 1, however, the decay time predicted by the Sabine reverberation equation does not approach zero; it approaches a constant. The dilemma of nonzero decay time for rooms with perfectly absorbing walls was investigated by researchers analyzing room acoustics in the 1930's and 1940's [49]-[52]. A remedy was proposed by Eyring [49] where he approximated the characteristic decay time

of these so-called “dead” rooms as

$$\tau = \frac{l_c}{-v \ln(1 - \alpha)} . \quad (07)$$

The parameter l_c is defined as the mean free path between reflections, and for a rectangular room is given by [54], [55], and [66]-[68]

$$l_c = \frac{4V}{S} . \quad (8)$$

This quantity is not the average distance between reflections for any given ray in the room; instead it is v times the reciprocal of the average reflection frequency (the average number of wall reflections per second). Note that the characteristic decay time given by Sabine, equation (6), and Eyring, equation (7), approaches the same value for small values of α . Recently, this so-called “dead” room formulation was used to analyze electromagnetic anechoic test chambers [69].

The “live” and “dead” room expressions given in this section are valid as long as reverberation is present in the room. Dunens and Lambert [56] have suggested that reverberation occurs when several wall reflections are present, and more importantly, they have shown that reverberation occurs after $8l_c/v$ to $10l_c/v$ seconds. For indoor wireless communications in rooms where the walls are not highly reflecting, energy propagates freely through walls of typical building materials, and as a result, few wall reflections occur. Before 10 l_c/c seconds elapses (where c is the speed of propagation of electromagnetic waves) only a minimal amount of energy is left in the room. The situation when few wall reflections are present in a cavity is referred to as a nonreverberated regime.

The study of acoustics concentrates primarily in units of energy. In wireless communication applications, however, the way in which the power level in a room decays with time (i.e., the power delay profile) is more important. By extending the concept presented in this section, it is possible to derive an expression for the average power delay profile of a room when relatively few wall reflections are present.

3. INDOOR POWER DELAY PROFILE MODEL (IPDP)

In developing the decay time for “dead” rooms in acoustics, Eyring assumed discontinuous drops in the power levels caused by wall reflections [49] and [55]. Using these same concepts, we developed an indoor power delay profile model. If an electromagnetic pulse is launched from a transmitter at some location, the received power at some other location in the room is depicted by Figure 3. After some time delay t_o , from the time the pulse leaves the transmitter, the power in the direct ray arrives at the receiver. The power level in the direct ray is usually the strongest signal and the time delay is given by $t_o = d/c$, where d is the separation distance of the receiver and transmitter, and c the speed of electromagnetic propagation in the room. This direct ray is illustrated by the thick arrow in Figure 3. The strength of this direct ray is P_o .

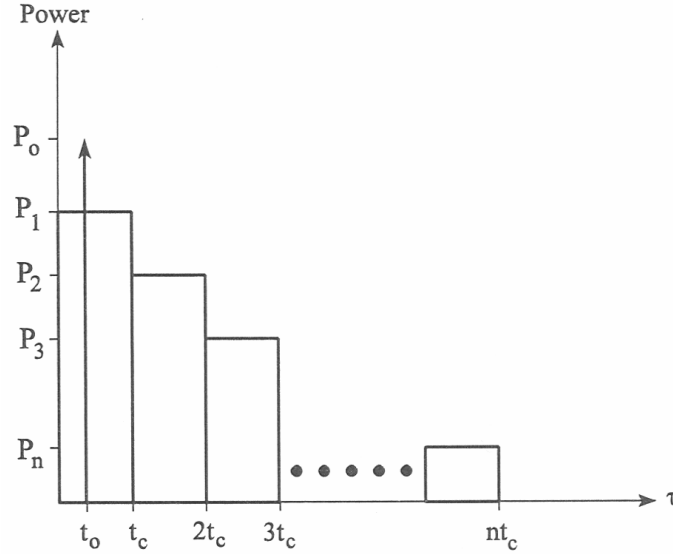


Figure 3. Typical field level distribution inside a room.

All the delayed components are due to reflections or scattering from objects such as walls, floor, ceiling, furniture, and people in the propagation path between the transmitter and receiver. To simplify this analysis, assume that the room is empty, such that all reflection originates from only the ceiling, floor, and walls. On average, after some given time delay t_c , all the pulses that make only one reflection off either the ceiling, floor, or walls, will arrive at the receiver. This time delay t_c is defined as the characteristic room time, and is formulated below. Pulses that arrive at the receiver after only one reflection have some mean power level P_1 . This power level is decreased from the transmitted power level by two primary attenuation factors. The first is simply the free-space loss proportional to $1/r^2$, where r is the path length that these rays travel. The second is the reduction in power due to reflection and absorption characteristics of the surfaces in the room. All pulses arriving after one reflection are represented in Figure 3 by the rectangular box with height P_1 and width t_c .

After some other time delay, or two characteristic times $2t_c$, it is assumed that all pulses arriving at the receiver would have made only two reflections. Pulses that arrive at the receiver after two reflections have some mean power level P_2 . This power level is a function of the path length and the reflection coefficient of two reflecting surfaces. It is assumed, on average, that pulses making two bounces will not arrive at the receiver until most of the pulses that make only one reflection have arrived. The rectangular box with height P_2 and width t_c in Figure 3 represents the pulses that arrive after two reflections. This process continues for additional reflections until the power levels are negligible. The series of rectangles in Figure 3 represent the pulses arriving at the receiver after n reflections with power levels given by P_n . As discussed below, the power delay profile is approximated by connecting the direct ray and the tops of the rectangular boxes representing the multipath components.

3.1 Characteristic Time t_c of a Room

The acoustic community uses the mean free path l_c as a means to determine characteristics about a room response. Actually, the quantity l_c/v is used as a means of estimating transience in a given room size. The characteristic time t_c of a room that is required before a given set of rays makes one reflection is assumed to be given by a function of the mean free path l_c , and by utilizing equation (8) can be expressed as

$$t_c = 2 \frac{l_c}{c} = \frac{8V}{cS} . \quad (9)$$

The justification of representing the characteristic time t_c in this manner is illustrated in Figure 4. Using a ray trace model, the arrival times were determined for rays making n bounces from the ceiling, floor, and walls in a room with a length of 6m, height of 3m, and width of 4m. Probability distribution curves verses arrival times for rays making n bounces are shown. The first plot corresponds to the distribution of arrival times for rays making only one bounce in the room. The remaining plots in Figure 4 correspond to the distribution of arrival times for rays making 2-10 bounces, respectively. Notice if a ray makes n bounces off reflecting surfaces, then by $t = nt_c$ the majority of the n -bounced rays have arrived at the receiver. That is to say, by $t = t_c$, most of the rays making one bounce arrive at the receiver; by $t = 2t_c$, most of the rays making two bounces arrive at the receiver, and so on for increasing number of bounces.

3.2 Reflected Power Levels

In both electromagnetic and acoustic reverberation rooms, the decay rate of energy is a function of the energy dissipated into the walls, floor, and ceiling through the parameter α ([45]-[55], [59]-[65], and [69]). The path length the rays travel is unimportant in the energy levels of reverberation cavities, because reverberation assumes the energy is uniformly distributed throughout the cavity. The model presented here attempts to predict the power delay profile for a situation where the room is not reverberant, which corresponds to the energy in the room not being uniformly distributed throughout the entire room. In fact, for most indoor wireless communication applications, the energy in the room will dissipate quickly and the reverberation conditions are rarely met. For this type of scenario, the power levels will be a function of the path lengths the rays travel, as well as the power dissipated in the reflecting surfaces.

It is possible to determine the path length and reflection coefficient of each ray striking a surface in a room using ray tracing approaches [16]-[29]. However, this approach as well as other numerical approaches [30]-[34] are time consuming. By using characteristic parameters of a room, it is possible to approximate the power levels at different times. The average power level of the bundle of rays that corresponds to rays after n reflections is approximated by

$$P_n = A \frac{\gamma^n}{d_{cn}^2} . \quad (10)$$

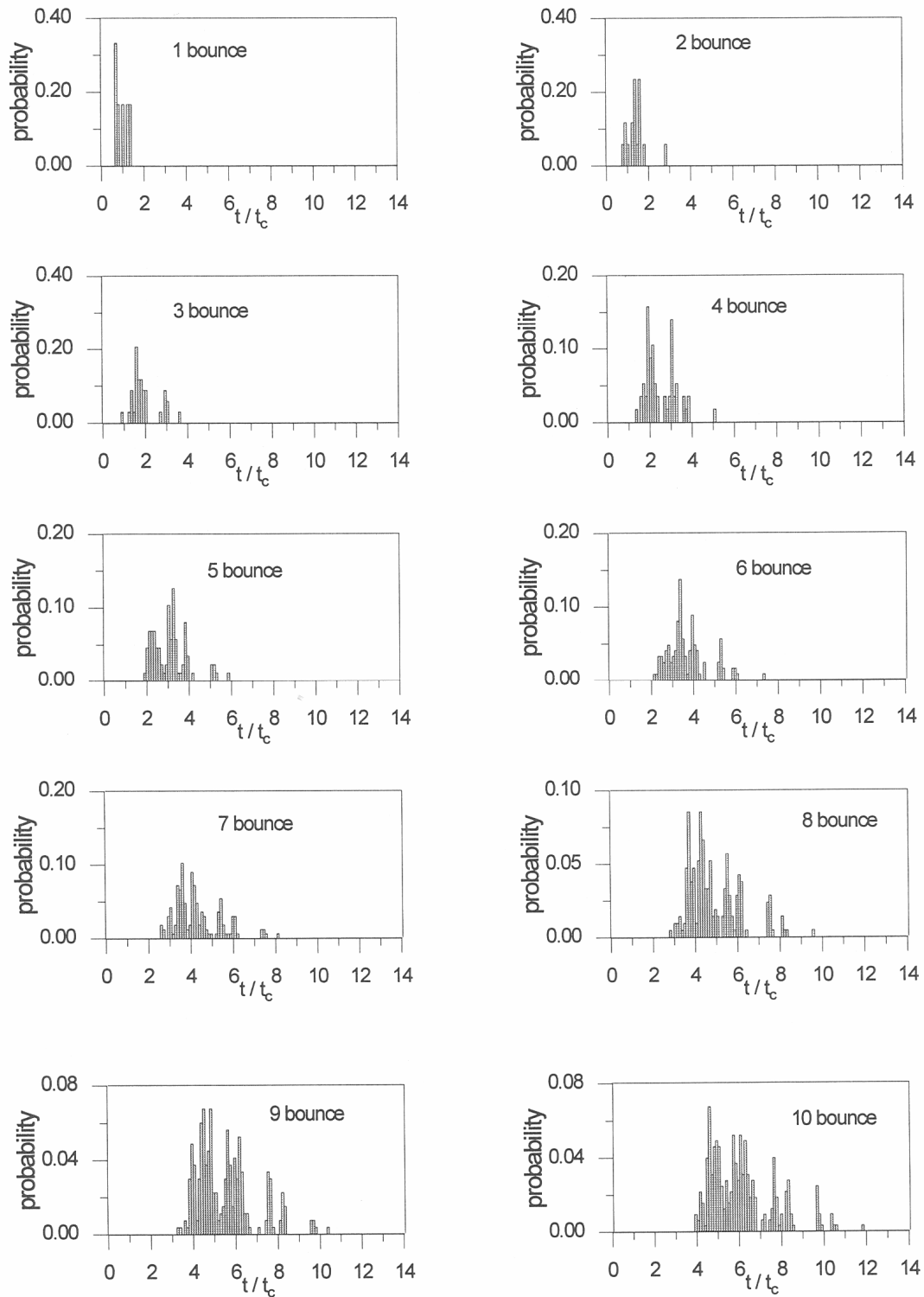


Figure 4. Probabilities of travel times of rays making n bounces.

A is a constant that is a function of the transmitting and receiving antennas and the transmitted power, and d_{cn} is the characteristic or effective distance that a bundle of rays making n reflections travels and is approximated by the time it takes these rays to reach the receiver (that is, some integer multiple of the characteristic time t_c). Using the definition of t_c given in equation (9), d_{cn} is expressed in terms of the characteristic length or mean free path l_c as

$$d_{cn} = n t_c c = 2 n l_c . \quad (11)$$

In equation (10), γ is the average power reflection coefficient. In general, it would be involved to determine the reflection coefficient from the incident angle and polarization of each ray in the room. Since we are only interested in the reflected power in an average sense, the average power reflection coefficient can be calculated in the same manner as is done in electromagnetic reverberation rooms [65] and [69]. Thus, the average power reflection coefficient is defined as

$$\gamma = 1 - \alpha , \quad (12)$$

where α is the average absorption coefficient of the surfaces in the rooms. It is calculated by averaging plane wave reflection coefficients over all possible angles of incidence and polarizations [65] and [69] and is expressed as

$$\alpha = 2 \int_0^{\pi/2} \left\{ 1 - \left[\frac{|R_{TM}(\theta)|^2 + |R_{TE}(\theta)|^2}{2} \right] \right\} \sin \theta \cos \theta d\theta , \quad (13)$$

where $R_{TE}(\theta)$ and $R_{TM}(\theta)$ are the plane-wave reflection coefficients for transverse electric and transverse magnetic waves, respectively. The plane-wave reflection coefficients are functions of the material properties, thickness of the reflection surfaces, and frequency of operation. Expressions for $R_{TM}(\theta)$ and $R_{TE}(\theta)$ can be found in [70]-[71].

3.3 Direct Ray

The direct ray arrives at the receiver at a time delay determined by the transmitter and receiver antenna separation d_o . The power level of the direct ray at the receiver is given by

$$P_o = \frac{A}{d_o^2} \quad (14)$$

where A is a constant. The antenna separation distance is known for a specific configuration, but the goal of this analysis is to determine the power delay profile of the room in an average sense; that is, to determine the global behavior of the room without knowing the exact location of the transmitter and receiver, or to determine the room average performance. Thus, it is assumed that on average, the direct path travels a distance equal to one characteristic length of the room $d_o = l_c$ and the direct ray arrives at the receiver at $t = t_o = l_c/c$.

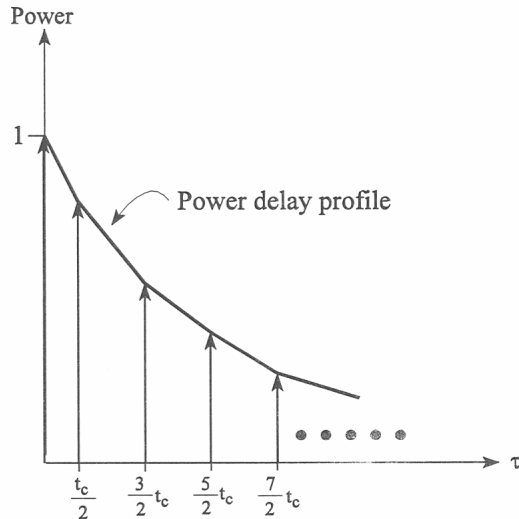


Figure 5. Normalized power delay profile (PDP) model for an indoor wireless radio propagation channel.

3.4 Power Delay Profile

With the power level and delay times of the direct ray and the reflection rays determined, the power delay profile (PDP) can be modeled. By initializing the delay time of the direct ray to zero and normalizing the power to P_o , the power levels at different delay times are approximated by

$$\begin{aligned} PDP_o &= 1 & \tau &= 0 & \text{for } n &= 0 \\ PDP_n &= \frac{1}{4} \frac{\gamma^n}{n^2} & \tau_n &= \frac{t_c}{2} (2n-1) & \text{for } n &\neq 0. \end{aligned} \quad (15)$$

This normalized power delay profile (PDP) is depicted in Figure 5. By connecting the arrows in this figure, an approximation to the power delay profile is obtained. One needs to keep in mind that this PDP is not for a particular location in a room; it corresponds to the average room behavior.

3.5 Room Consisting of Different Reflecting Surfaces

The average reflected power calculated from equation (12) assumes that all the reflecting surfaces are identical. When different reflecting surfaces are present in a room the average power reflection coefficient is calculated as a weighted average of all the surfaces, similar to what is done in acoustic and electromagnetic cavities [49] and [69]. The effective average absorption and the consequent average power reflection coefficient in a room with different reflecting surfaces is given by

$$\begin{aligned} \alpha_{eff} &= \frac{\sum S_n \alpha_n}{S} \\ \gamma_{eff} &= 1 - \alpha_{eff}, \end{aligned} \quad (16)$$

where S is the total surface area of the room, S_n is the area of surface n , and α_n is the average absorption of surface n .

4. GEOMETRY AND MATERIAL PROPERTIES VARIATIONS

The IPDP model was implemented to investigate the effects of variable room size and material properties of the surfaces (or walls) on the power delay profile. The first example illustrates the effects of room size. Figure 6 shows the PDP for a room 4 m wide, 3 m high, and 6 m long. The surfaces (walls, ceiling, and floor) in this room are composed of an infinitely thick, homogenous concrete slab with $\epsilon_r = 3$, $\sigma = 0.01$ S/m. Also shown in this figure are results for the same surfaces with the dimensions of the room doubled and halved. These results are obtained for a frequency of 1.5 GHz. For all three of these rooms, the average absorption and reflection coefficients of the surfaces are $\alpha = 0.88$ and $\gamma = 0.12$. These results illustrate, as one might expect, that for the large room, the energy rings longer. This results in the power levels remaining relatively high for long periods of time. For the smallest room dimension, the power levels decay relatively quickly.

The effects of different material properties of the surfaces were also investigated. Figure 7 shows the PDP for a room 4 m wide, 3 m high, and 6 m long. The surfaces in this room are assumed to be infinitely thick and homogenous with $\epsilon_r = 3$, $\sigma = 0.01$ S/m ($\alpha = 0.88$ and $\gamma = 0.12$). Also shown in this figure are results for the same room size with the conductivities increased to $\sigma = 0.1$ S/m ($\alpha = 0.86$ and $\gamma = 0.14$) and $\sigma = 1.01$ S/m ($\alpha = 0.58$ and $\gamma = 0.42$). Other results shown in this figure are for the same size room with $\epsilon_r = 2$, $\sigma = 0.0$ S/m ($\alpha = 0.92$ and $\gamma = 0.08$) and $\epsilon_r = 1.2$, $\sigma = 0.0$ S/m ($\alpha = 0.98$ and $\gamma = 0.02$). When the reflections from the surfaces are large, the field strength in the room remains relatively high for long periods of time, illustrated by $\sigma = 1.0$ S/m ($\alpha = 0.58$ and $\gamma = 0.42$). On the other hand, when the reflections from the surfaces are small, the field strength in the room will decay relatively quickly in a short period of time, illustrated by $\epsilon_r = 1.2$, $\sigma = 0.0$ S/m ($\alpha = 0.98$ and $\gamma = 0.02$).

Finally, the effect of surfaces consisting of different materials was investigated. In the three examples investigated, it was assumed that the material properties of the ceiling are different from the other reflecting surfaces in the room. For this condition, the effective absorption coefficient given by equation (16) reduces to the following for a room for the two types of reflecting surfaces

$$\alpha_{eff} = \alpha_{w,f} \frac{S - S_c}{S} + \alpha_c \frac{S_c}{S}, \quad 17$$

where S is the total surface area of the room, S_c is the surface area of the ceiling, α_c is the average absorption coefficient of the ceiling, and $\alpha_{w,f}$ is the average absorption coefficient of the walls and floor. In the first example, it was assumed that all the reflecting surfaces (including the walls, floor and ceiling) are composed of the same material ($\epsilon_r = 3$, $\sigma = 0.01$ S/m) and are of infinite thickness. When all the surfaces in the room are the same, the average absorption and reflection for the room can be calculated by equations (12) and (13) and are $\alpha_{w,f,c} = 0.88$ and $\gamma_{w,f,c} = 0.12$. In the second example, it was assumed that the ceiling of the room is perfectly absorbing (i.e., $\alpha_c = 1.0$ and $\gamma_c = 0.0$) and the walls and floor have the same material as in the first example (i.e., $\alpha_{w,f} = 0.88$ and $\gamma_{w,f} = 0.12$). The last example corresponds to a room with a ceiling that is perfectly reflecting (i.e., $\alpha_c = 0.0$

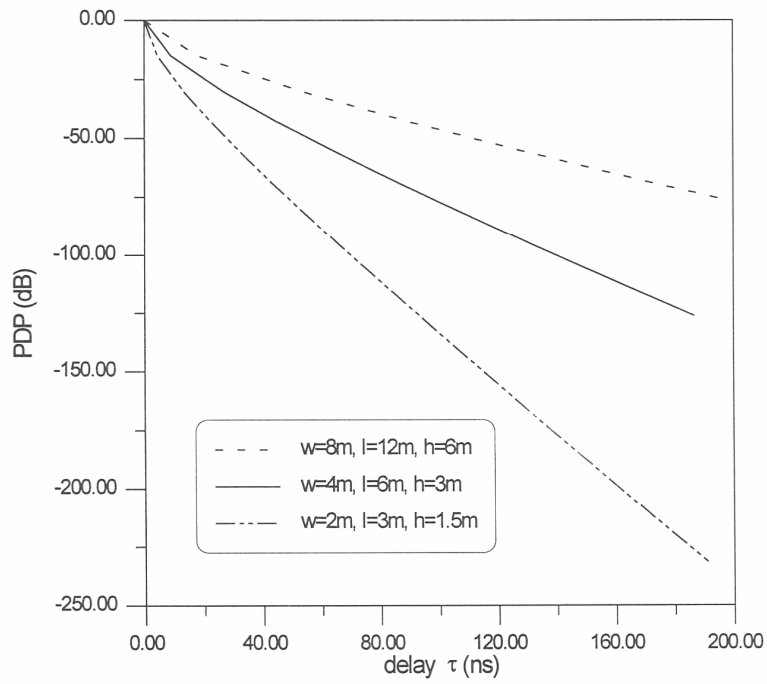


Figure 6. Variations of the PDP for different size rooms.

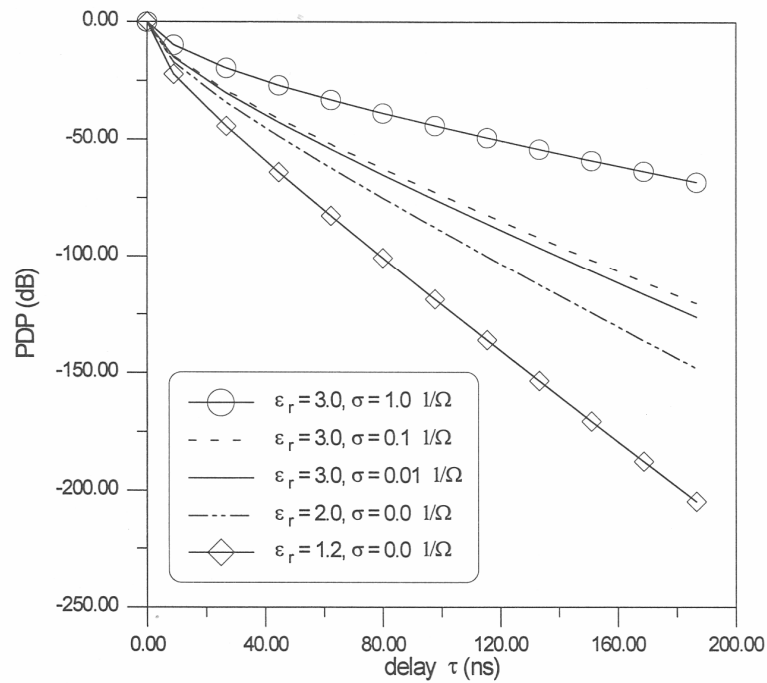


Figure 7. Variations of the PDP for a room 4 m wide, 3 m high, and 6 m long for different types of wall materials.

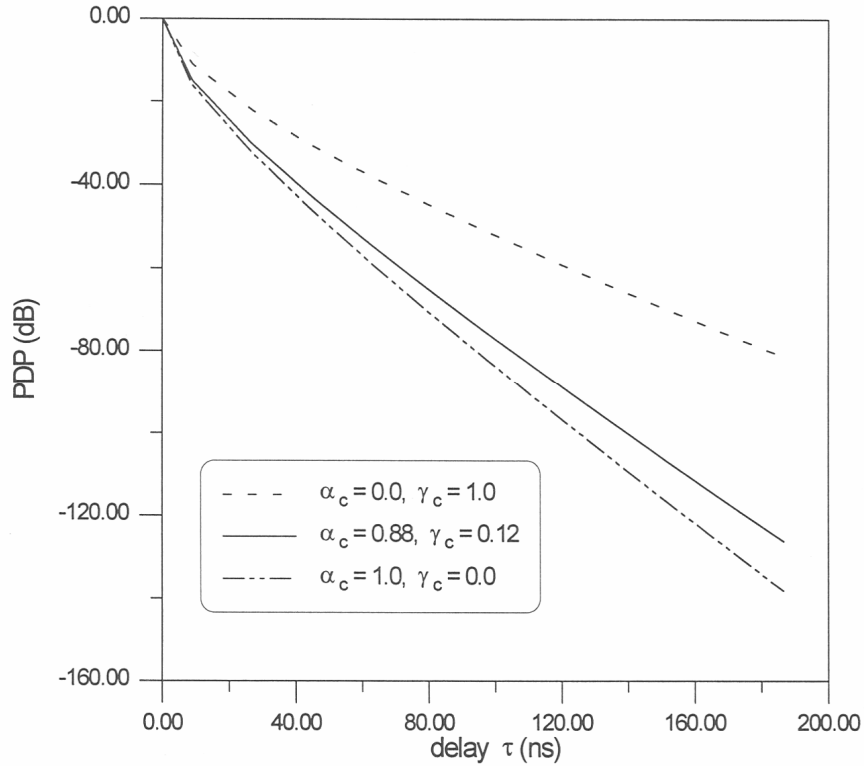


Figure 8. Variations of the PDP for a room with different materials in the ceiling.

and $\gamma_c = 1.0$) and the walls and floor have the same material as in the first example (i.e., $\alpha_{w,f} = 0.88$ and $\gamma_{w,f} = 0.12$). The results of all three of these examples are shown in Figure 8. Similar results were obtained for the situation where one wall has different properties than the remaining walls, floor, and ceiling. These results are shown in Figure 9. These two figures illustrate how the field levels in a room vary as the properties of one of the reflecting surfaces in a room change. As expected, as γ_{eff} increases, the power levels in the room remain at relatively high levels for longer periods of time.

5. WIDEBAND SYSTEMS

The IPDP model presented here has a frequency dependence due to the average reflected power being a function of the reflection coefficient of the reflecting surfaces. These reflection coefficients are functions of the material properties, surface (or wall) thickness, and frequency. The question that arises is: what frequency should be used when a system has a given bandwidth? Figure 10 shows results of γ for different types of surfaces at various frequencies. If γ does not vary appreciably in the given bandwidth, then the value of γ at the carrier frequency can be used. However, for some materials and wall geometries, γ can exhibit a strong resonant behavior in a given bandwidth (see the solid curve in Figure 10). By using the maximum average reflected power γ_{max} in the given bandwidth, a worse case or upper limit on the decay rate is obtained since the IPDP model is directly related to the value of

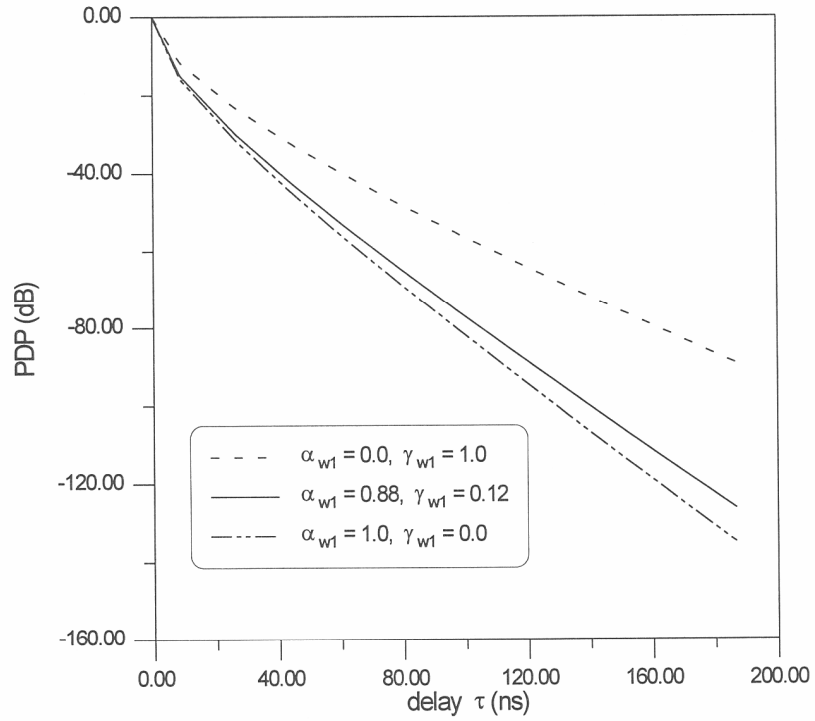


Figure 9. Variations of the PDP for a room with different materials in one wall.

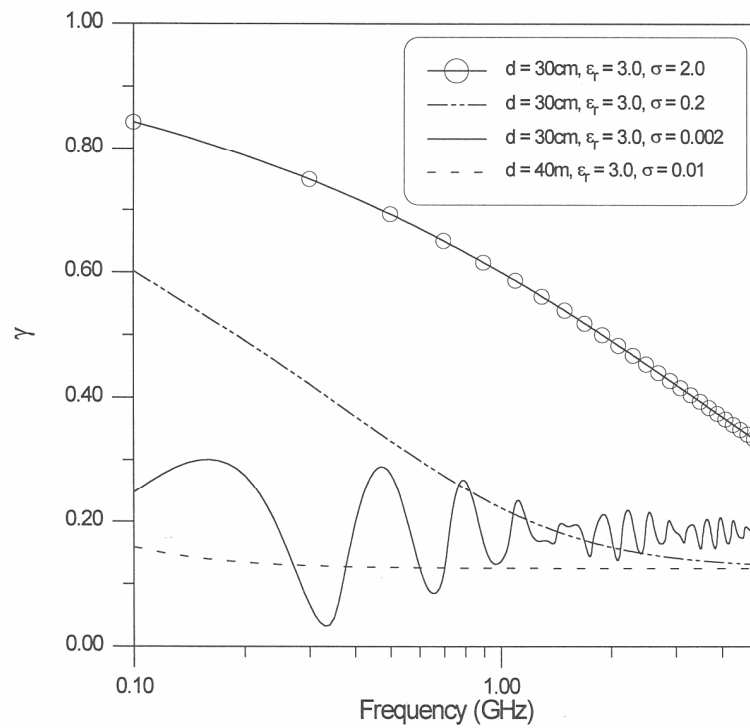


Figure 10. Variations of γ for a room with different types of reflecting surfaces.

γ . Thus, to calculate the power delay profile for a wide bandwidth system, γ is calculated for the entire bandwidth and the maximum average reflected power γ_{max} is used.

6. VALIDATION OF THE MODEL

We validated the power delay profile model by comparing it to results obtained from a finite-difference time-domain (FDTD) model and measured data. We are investigating the use of a three-dimensional finite-difference time-domain (FDTD) approximation to Maxwell's curl equations to determine the impulse response of the indoor channel. The FDTD technique requires the volume of the room and the walls to be subdivided into unit cubic cells. The electric and magnetic field vector components on these cells are represented by a Yee space lattice [72]. With this space lattice, the Yee algorithms ([72] and [73]) for the coupled Maxwell's curl equations can be used to solve for both the electric and magnetic fields in time and space. The electric and magnetic fields for the x component are given by

$$\begin{aligned} E_x^{n+1}(i+1/2, j, k) &= E_x^n(i+1/2, j, k) + \frac{\Delta t}{\epsilon \Delta h} F_H \\ H_x^{n+1/2}(i, j+1/2, k+1/2) &= H_x^{n-1/2}(i, j+1/2, k+1/2) + \frac{\Delta t}{\mu \Delta h} F_E \end{aligned} \quad (18)$$

Similar equations exist for the other components of the electric and magnetic fields. In the above equations, F_H is an expression that contains sums and differences of the orthogonal H field components around the $E_x(i+1/2, j, k)$ field, and F_E is an expression that contains sums and differences of the orthogonal E field components around the $H_x(i, j+1/2, k+1/2)$ field [72] and [73]. In these equations, E^{n+1} corresponds to the electric fields at the new (or current) timestep, E^n corresponds to the electric fields at the previous timestep, $H^{n+1/2}$ corresponds to the current magnetic fields (calculated with E^n), $H^{n-1/2}$ corresponds to the magnetic fields at the previous timestep, Δh is the cell size, and Δt is the timestep. Note that the electric and magnetic field components are staggered in both space and time in order to achieve a compact but explicit central difference scheme.

The finite-difference equation first advances all the magnetic fields in the entire volume one time step by using the electric fields at the previous time step (E^n). Then, the electric fields are advanced by using the magnetic fields that were just calculated. For stability of this scheme, one needs to ensure that

$$\Delta t < \frac{\Delta h}{c\sqrt{3}}. \quad (19)$$

This criterion is referred to as the Courant or the CFL (Courant-Friedrick-Lewy) stability condition [74] and [75], and essentially states that the numerical speed of propagation must exceed the physical speed of propagation for numerical stability.

The finite-difference grid was continued three spatial cells beyond the outer edges of the walls, and the grid was terminated at that point by an absorbing boundary condition. A 16-cell thick Berenger perfectly matched layer with a quadratic conductive profile was used as the absorbing boundary condition [76].

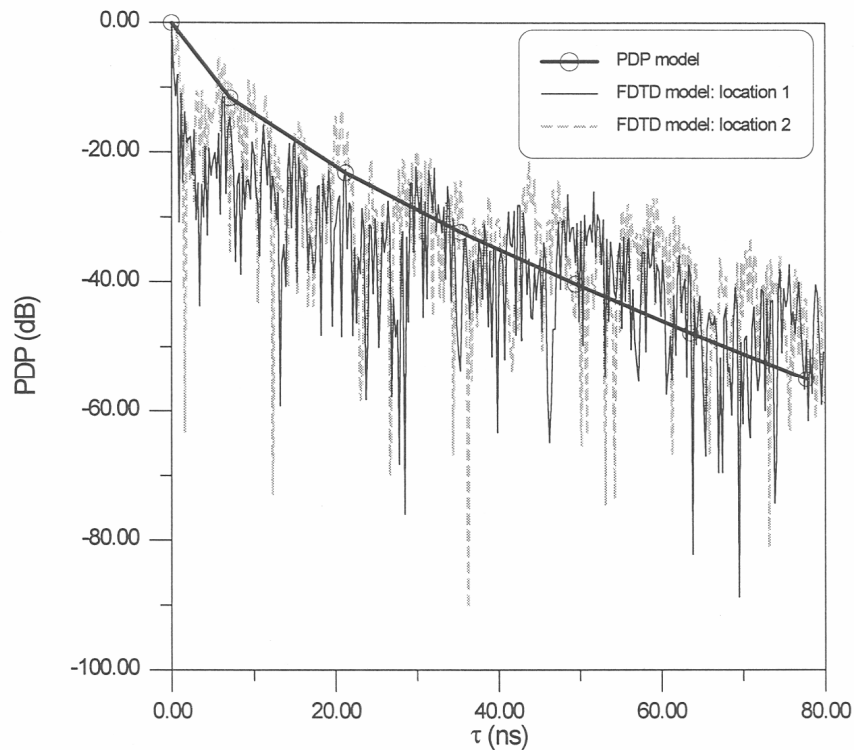


Figure 11. Comparison of the IPDP model to the FDTD simulation for a room with a length of 5.4 m, a width of 3.3 m, and a height of 2.4 m, assuming the walls are 30 cm thick with $\epsilon_r = 3.0$ and $\sigma = 0.01$ S/m.

Figure 11 shows the results of the predicted power delay profile for two different locations in a room obtained from the FDTD simulation. The current source waveform used in this simulation corresponded to a first derivative of a Gaussian pulse. The results in the figure correspond to a room 2.4 m high, 3.3 m wide, and 5.4 m long and the walls, floor, and ceiling for this room have a thickness of 30 cm with $\epsilon_r = 3.0$ and $\sigma = 0.01$ S/m. Also shown in this figure are corresponding results from the IPDP model. Figure 12 shows a comparison of the IPDP model and the FDTD model for a room with the same dimensions and with the conductivity increased to 2.0 S/m. The comparisons in these two figures illustrate that the IPDP model predicts the same decay characteristics in the power delay profile as predicted from the FDTD model.

Finally, comparisons to measured data are presented. Our Institute has developed an impulse measurement system to measure the power delay profile for an indoor propagation channel. This system is based on a correlation technique using a pseudorandom transmitted code and is detailed in [77]-[78]. This system measures a bandlimited impulse response at a carrier frequency of 1.5 GHz with bandwidth of 500 MHz. The power delay profile was measured in two different rooms. The first room is a small office with a height of 3.20 m, a width of 2.31 m, and a length of 5.26 m. The second room is a laboratory with a height of 5.0 m, a width of 7.18 m, and a length of 9.35 m. The walls in the office and laboratory

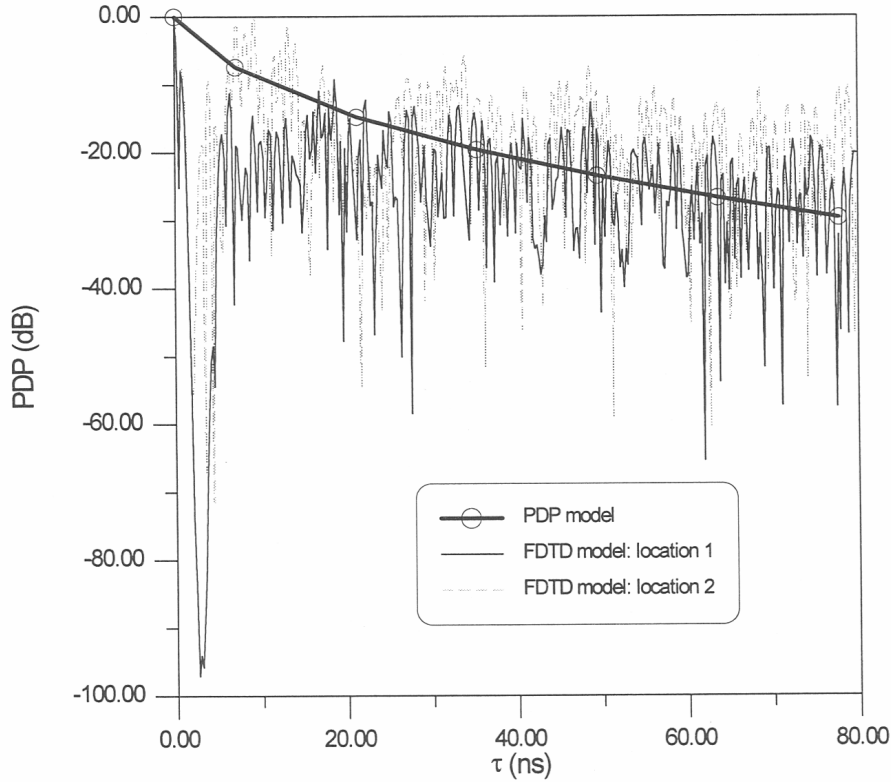


Figure 12. Comparison of the IPDP model to the FDTD simulation for a room with a length of 5.4 m, a width of 3.3 m, and a height of 2.4 m, assuming the walls are 30 cm thick with $\tau_r = 3.0$ and $l = 2.0$ 81m.

were composed of concrete slabs and concrete blocks of thickness 14.5 cm with $\epsilon_r = 6.0$, $\sigma = 1.95 \cdot 10^{-3}$ S/m [79].

Figures 13 and 14 show comparisons of the IPDP model to measured data for these two rooms. The measured data in both rooms were obtained with the transmitter located near a corner of their respective room at a height of 1.8 m and the receiver was placed on a cart with an antenna height of 1.8 m. Location 1 in Figures 13 and 14 corresponds to the receiver placed at a location near one of the walls of the respective rooms, and location 2 in the two figures corresponds to the receiver placed at the center of the respective rooms. Location 3 in Figure 14 corresponds to the transmitter being placed at the center of the laboratory and the receiver placed 2 m from one of the walls. The comparisons in these two figures illustrate that the IPDP model predicts the same decay characteristics in the power delay profile as seen in the measurements.

With the receiver placed on a moveable cart, the impulse responses for several locations distributed throughout the rooms were obtained. The magnitude of all of the impulse responses in each of the two rooms were averaged together to obtain an effective average power delay profile of each room. The results of these averages along with the results of the IPDP model are shown in Figures 15 and 16 for the office and laboratory, respectively.

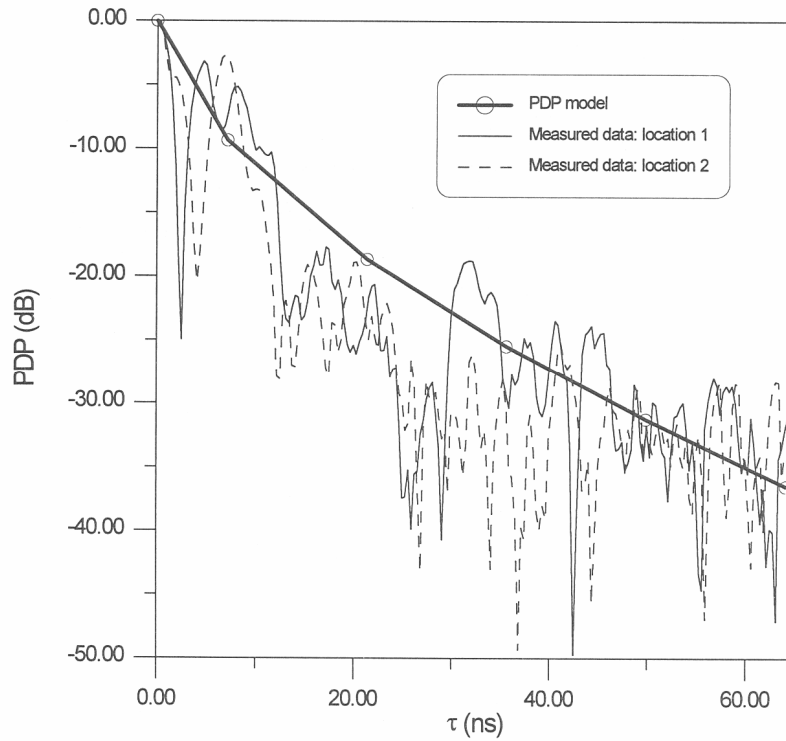


Figure 13. Comparison of the IPDP model to measured data for a small office with a length of 5.26 m, a width of 2.31 m, and a height of 3.20 m.

The comparisons in these two figures illustrate once again that the IPDP model predicts the same decay characteristics in the power delay profile as seen in the measurements.

The results of the IPDP model can be used to estimate the rms delay spread for these two rooms. The rms delay spread is calculated by the following expression [1] and [4]:

$$\tau_{rms} = \left[\frac{\int (t - D)^2 PDP(t) dt}{\int PDP(t) dt} \right]^{1/2}$$

where

$$D = \frac{\int t PDP(t) dt}{\int PDP(t) dt} .$$

Using the results of our model, we estimated a rms delay spread of 6.1 ns for the office and 13.2 ns for the laboratory. The rms delay spread was also calculated from the measured data. For the office, the rms delay spread for locations 1 and 2 were calculated to be 7.5 ns and 5.9 ns, respectively. From the measured average power delay profile of the office (see Figure 15), the rms delay spread was calculated to be 7.5 ns. For the laboratory, the rms delay spread for locations 1, 2, and 3 was calculated to be 14.7 ns, 12.5, and 15.1 ns, respectively. From the measured average power delay profile of the laboratory (see Figure 16), the rms delay spread was calculated to be 15.6 ns. The rms delay spread obtained from the measured data of the two different rooms compares well to the delay spread obtained from

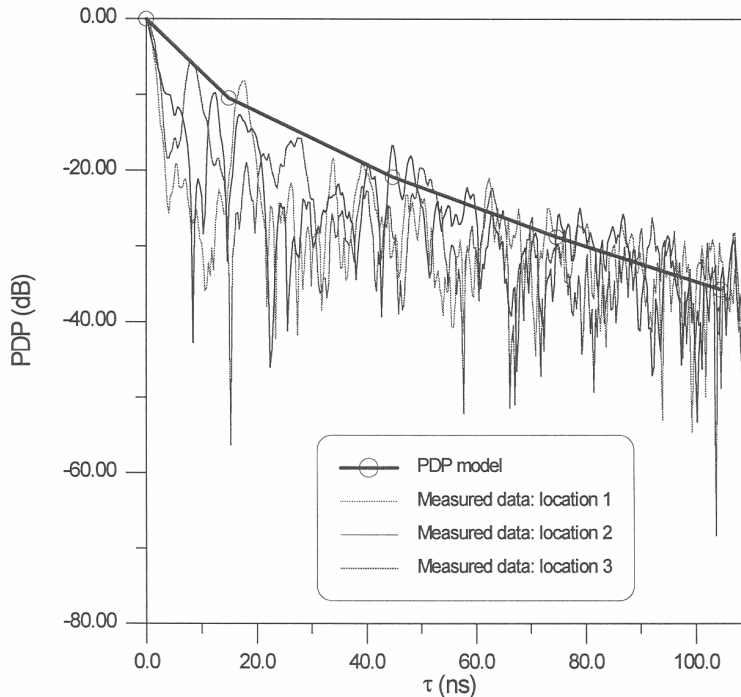


Figure 14. Comparison of the IPDP model to measured data for a laboratory with a length of 9.35 m, a width of 7.18 m, and a height of 5.00 m.

the model. Keeping in mind that the IPDP model in its present form neglects the energy propagation through doors and windows, and scattering and reflections from lights fixtures, air-conditioning units, and piping (which were present in these two rooms), we conclude that the IPDP model agrees well to measured data in predicting the room power delay profile characteristics.

7. DISCUSSION AND CONCLUSION

In this paper, we present a model for predicting the characteristics of the power delay profile of an indoor wireless propagation channel. This IPDP model is based on simple room parameters: room volume, surface area, and the average power reflected from surfaces in the room. Comparisons to FDTD results and to measured data are presented. From these comparisons it was demonstrated that the IPDP model can be used to predict the decay characteristics of the power delay profile and estimated the rms delay spread within a room.

The IPDP model does not give a detailed description of a room impulse response. The intent of this model is to give a global (or average) behavior of the channel for the system placed in an arbitrary room location. The advantage of this IPDP model is that it is based on simple assumptions, so the power delay profile within a room can be calculated in a matter of seconds on a personal computer. Hence, the IPDP model can be used to quickly

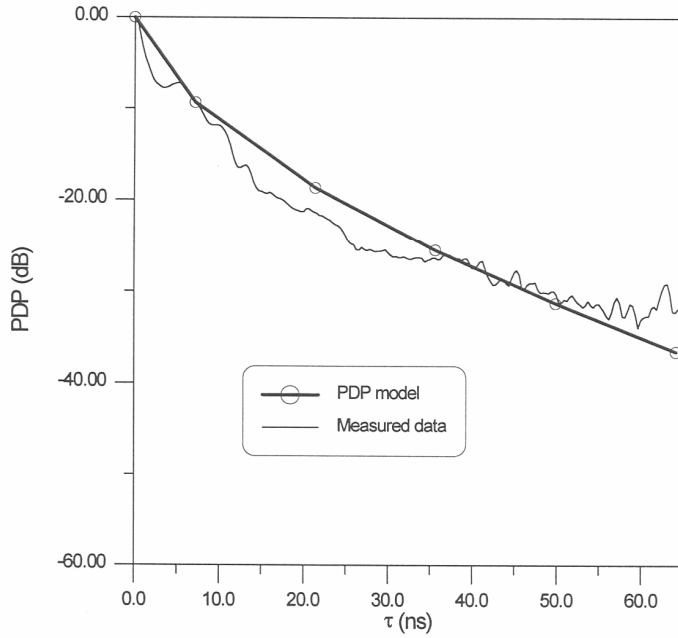


Figure 15. Comparison of the IPDP model to the measured data obtained by averaging several locations through the office with a length of 5.26 m, a width of 2.31 m, and a height of 3.20 m.

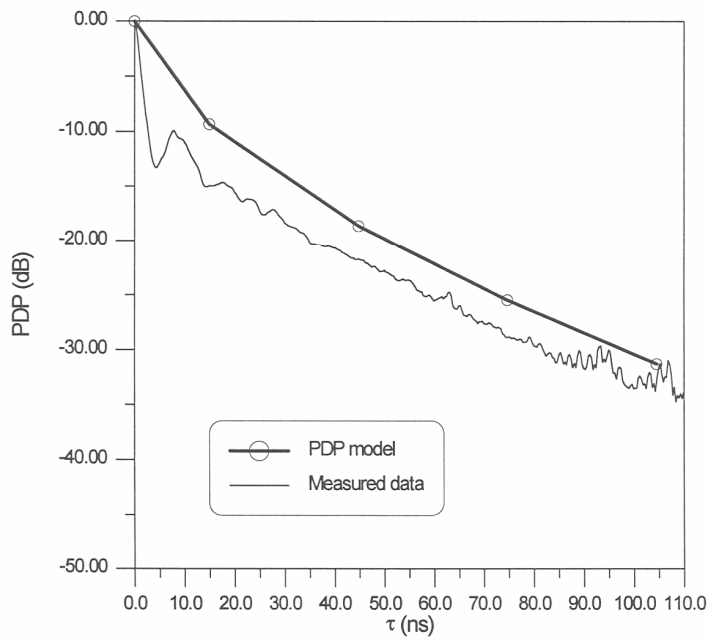


Figure 16. Comparison of the IPDP model to the measured data obtained by averaging several locations through the laboratory with a length of 9.35 m, a width of 7.18 m, and a height of 5.00 m.

assess the average response of a room. Further, the IPDP model is a time-efficient means for approximating the rms delay spread and consequent ISI of a specified wireless indoor channel. The IPDP model was used to estimate the rms delay spread and comparison to the measured data show good correlation.

The IPDP model presented here is valid until reverberation occurs in the room. Dunens and Lambert [56] have shown that reverberation occurs after $8l_c/v$ to $10l_c/v$ seconds, which suggests that the model presented here will predict the decay rate of the PDP for times less than five characteristic room times (that is, $t < 5t_c$). For $t > 5t_c$, modifications are required for this model to account for room reverberation. For most applications (rooms with highly absorbing walls) the energy in a room decays to minimal levels before reverberation can occur. However, wireless links are being implemented in places with highly conducting walls (i.e., metal warehouses and shipboard communications). Under these types of propagation environments, the model presented here must be combined with the reverberation decay rate approaches [59]-[64] and [69]. The combination of these two approaches is presently being investigated for shipboard communication.

Future work will also include predicting the power delay profiles of coupled or adjacent rooms and accounting for the leakage of energy through doors and windows. Other areas of future work are the effects of furniture in the room and the effects of realistic antenna patterns. It is believed that the effects of narrow beam antenna patterns can be incorporated into the model by weighting the angle dependence of the average reflection given in equation (13), but this is still being investigated.

While the model presented here is simple to implement, it does require knowing material properties and geometries of the reflecting walls in the room. Until recently [80]-[84], little effort has been given to characterizing building materials. More work in this area is needed, not just for this model, but for all types of indoor field strength prediction models and for impulse response models.

8. ACKNOWLEDGMENTS

The authors would like to thank Y. Lo and P. Papazian of the Institute for Telecommunication Sciences for supplying measured impulse response data. We also thank K.C. Allen of the Institute for Telecommunication Sciences and D.A. Hill of the National Institute of Standards and Technology for their helpful discussions.

9. REFERENCES

- [1] J.C.I. Chuang, "The effects of time delay spread on portable radio communication channels with digital modulation," *IEEE J. Selected Area Commun.*, vol. 5, no. 5, pp. 879-889, 1987.
- [2] P.A. Bello and B.D. Nelin, "The effect of frequency selective fading on the binary error probabilities of incoherent and differentially coherent matched filter receivers," *IEEE Trans. Commun. Systems*, Jun., pp. 170-186, 1963.
- [3] M. Wittmann, J. Marti, and T. Kürner, "Impact of the power delay profile shape on the bit error rate in mobile radio systems," *IEEE Trans. on Veh. Technol.*, vol. 26, no. 2, pp. 329-339, 1997.
- [4] D.M.J. Devasirvatham, "Multipath time delay spread in the digital portable radio environment," *IEEE Commun. Mag.*, vol. 25, no. 6, pp. 13-21, 1987.
- [5] L.J. Greenstein and V.K. Prabhu, "Analysis of multipath outage with applications to 90-Mbits/s PSK systems at 6 and 11 GHz," *IEEE Trans. Commun.*, vol. 27, no. 1, pp. 68-75, 1979.
- [6] R.C.V. Macario (Ed), *Modern Personal Radio Systems*. London: Institution of Electrical Engineers, 1996, chapter 3.
- [7] C.A. Siller, Jr., "Multipath propagation," *IEEE Commun. Mag.*, vol. 22, no. 2, pp. 6-15, 1984.
- [8] K. Pahlavan and A.H. Levesque, *Wireless Information Networks*. New York: John Wiley & Sons, 1995, chapter 8.
- [9] T.S. Rappaport, *Wireless Communications: Principles and Practice*. Upper Saddle River, N.J.: Prentice Hall PTR, 1996, chapter 5.
- [10] W.C. Jakes, "An approximate method to estimate an upper bound on the effect of multipath delay distortion on digital transmission," *IEEE Trans. Commun.*, vol. 27, no. 1, pp. 76-81, 1979.
- [11] S.U.H. Qureshi, "Adaptive equalization," *Proc. IEEE*, vol. 53, pp. 1349-1387, 1985.
- [12] R. Steele (Ed), *Model Radio Communications*. New York: IEEE Press, 1995, chapters 6 and 8.
- [13] W.C. Jakes (Ed), *Microwave Mobile Communications*. New York: IEEE Press, 1993, chapters 5 and 6.
- [14] P.L. Perini and C.L. Holloway, "Angle and space diversity comparisons in different mobile radio environments," *IEEE Trans. on Antennas and Propag., special issue on wireless communications*, vol. 46, no. 6, pp. 764-775, 1998.

- [15] L. Boithias, *Radio Wave Propagation*. New York: McGraw-Hill Book Company, 1987, chapter 6.
- [16] M.C. Lawton and J.P. McGeehan, "The application of GTD and ray launching techniques to channel modelling for cordless radio systems," in *Proc. 42nd IEEE Veh. Technol. Conf.*, Denver, CO, 1992, pp. 125-130.
- [17] A.J. Rustako, Jr., N. Amitary, G.J. Owens, and R.S. Roman, "Radio propagation at microwave frequencies for line-of-sight micro cellular mobile and personal communications," *IEEE Trans. Veh. Technol.*, vol. 40, no. 1, pp. 203-210, 1991.
- [18] G. Bronson, K. Pahlavan, and H. Rotithor, "Performance prediction of wireless LANs based on ray tracing algorithms," in *Proc. PIMRC 93*, Yokohama, Japan, 1993, pp. 151-156.
- [19] G. Yang and K. Pahlavan, "Analysis of multicarrier modems in an office environment using 3D ray tracing," in *Proc. IEEE GLOBECOM 94*, San Francisco, CA, 1994, pp. 42-46.
- [20] S.Y. Seidel and T.S. Rappaport, "A ray tracing technique to predict path loss and delay spread inside building," in *IEEE GLOBECOM 92*, Orlando, FL, 1992, pp. 649-653.
- [21] W. Honcharenko, H.L. Bertoni, J.L. Dailing, J. Qian, and H.D. Yee, "Mechanisms Governing UHF propagation on single floors in modern office buildings," *IEEE Trans. Veh. Technol.*, vol. 41, no. 4, pp. 496-504, 1992.
- [22] T. Holt, K. Pahlavan, and J.F. Lee, "A graphical indoor radio channel simulator using 2D ray tracing," in *Proc. of 3rd IEEE Int. Symp. on Personal, Indoor and Mobile Radio Commun.*, Boston, MA, 1992, pp. 411-416.
- [23] J.W. McKown and R.L. Hamilton, Jr., "Ray tracing as a design tool for radio networks," *IEEE Network Mag.* vol. 5, no. 6, pp. 27-30, 1991.
- [24] R.A. Valenzuela, "A ray tracing approach to predicting indoor wireless transmission," in *Proc. IEEE Vehicular Technology Conf.* Secaucus, NJ, 1993, pp. 214-218.
- [25] U. Dersch, J. Troger, and Ernst Zollinger, "Multiple reflections of radio waves in a corridor," *IEEE Trans. on Antennas and Propagat.*, vol. 42, no. 9, pp. 1571-1574, 1994.
- [26] S.H. Chen and S.K. Jeng, "An SBR/Image approach to indoor radio wave propagation in indoor environments with metallic furniture," *IEEE Trans. on Antennas and Propagat.*, vol. 45, no. 1, pp. 98-106, 1997.
- [27] S.Y. Seidel and T.S. Rappaport, "Site-specific propagation prediction for wireless in-building personal communication system design," *IEEE Trans. on Veh. Technol.*, vol. 43, no. 4, pp. 879-891, 1994.

- [28] S.Y. Tan and H.S. Tan, "Modelling and measurements of channel impulse response for an indoor wireless communication systems," *IEE Proceeding on Microwave, Antennas, and Propagat.*, vol. 142, no. 6, pp.405-410, 1995.
- [29] P. Kreuzgruver, P. Unterberger, and R. Gahleitner, "A ray splitting model for indoor radio propagation associated with complex geometries," in *Proc. IEEE Vehicular Technology Conf.*, Secaucus, NJ, 1993, pp. 227-230.
- [30] L. TaIbi and G.Y. Delisle, "Finite difference time domain characterization of indoor radio propagation," in *Electromagnetic Waves Pier 12, Progress in Electromagnetic Research*, J. A. Kong (ED). Cambridge, Massachusetts: EMW Publishing, 1996, pp. 251-275.
- [31] A. Lauer, I. Wolff, A. Bahr, J. Pamp, J. Kunisch, and I. Wolff, "Mutli-mode FDTD simulations of indoor propagation including antenna properties," in *Proc. 1995 IEEE 45th Vehicular Technology Conference*, Chicago, IL, 1995, pp. 454-458.
- [32] C.L. Holloway, M.G. Cotton, and P. McKenna, "A simplified model for calculation the decay rate of the impulse response for an indoor propagation channel," in *Proc. 2nd Annual Wireless Communications Conference* Boulder, CO., 1997, pp. 210-214.
- [33] G. Yang, K. Pahlavan, and J.F. Lee, "A 3D propagation model with polarization characteristics in indoor radio channels," in *Proc. IEEE GLOBECOM 93*, Houston, TX, 1993, pp. 1252-1256.
- [34] L. TaIbi and G. Delisle, "Wideband propagation measurements and modeling at millimeter wave frequencies," in *Proc. IEEE GLOBECOM 94*, San Francisco, CA, 1994, vol. 1, pp. 47-51.
- [35] A.A.M. Saleh and R.A. Valenzuela, "A statistical model for indoor multipath propagation," *IEEE J. Selected Areas Commun.*, vol. 5, no. 2, pp. 128-137, 1987.
- [36] D. Molkdar, "Review on radio propagation into and within buildings," *IEE Proc. H: Microwave, Antennas and Propagation*, vol. 138, no. 1, pp. 61-73, 1991.
- [37] R. Ganesh and K. Pahlavan, "Modeling of the indoor radio channel," *IEE Proc. I: Commun. Speech and Vision*, vol. 139, no. 5, pp. 153-161, 1991.
- [38] R. Ganesh and K. Pahlavan, "Statistics of short time and spatial variations measured in wideband indoor radio channels," *IEE Proc. H: Microwave, Antennas and Propagation*, vol. 140, no. 4, pp. 297-302, 1993.
- [39] T.S. Rappaport, S.Y. Seidel, and K. Takamizawa, "Statistical channel impulse response models for factory and open plan building radio communication system design," *IEEE Trans. Commun.*, vol. 39, no. 5, pp. 794-807, 1991.
- [40] P. Yegani and C.D. McGillem, "A statistical model for the factory radio channel," *IEEE Trans. Commun.*, vol. 39, no. 10, pp. 1445-1454, 1991.

- [41] H. Hashemi, "Impulse response modeling of indoor radio propagation channels," *IEEE J. Selected Areas Commun.*, vol. 11, no. 7, pp. 967-978, 1993.
- [42] G.A. Hufford, "A characterization of the multipath in the HDTV channel," vol. 38, no. 4, pp. 252-254, 1992.
- [43] R.A. Dalke, G.A. Hufford, R.L. Ketchum, "A digital simulation model for local multipoint and multichannel multipoint distribution services," NTIA Report 97-340, NTIA/ITS, U.S. Department of Commerce, Boulder, CO., Jul. 1997.
- [44] K. Pahlavan and S.J. Howard, "Statistical AR models for the frequency selective indoor radio channels," *IEE Electr. Lett.*, vol. 26, no. 15, pp. 1133-1135, 1990.
- [45] W.C. Sabine, *Collected Papers on Acoustics*. New York: Dover, 1964.
- [46] K Buckingham, "Theory and interpretation of experiments on the transmission of sound through partition walls," *Scientific Papers of the Bureau of Standards*, vol. 20, pp. 193-219, 1924-1926.
- [47] R.F. Norris, "Application of Norris-Andree method of reverberation measurement to measurements of sound absorption," *J. Acoustical Soc.*, vol. 4, pp. 361-370, 1993.
- [48] R.W. Young, "Sabine reverberation equation and power calculations," *J. Acoustical Soc. of America*, vol. 31, no. 7, pp. 912-921, 1959.
- [49] C.F. Eyring, "Reverberation time in DEAD rooms," *J. Acoustical Soc.*, vol. 1, pp. 217-241, 1930.
- [50] P.M. Morse and R.H. Bolt, "Sound waves in rooms," *Rev. of Modern Phy.*, vol. 16, no. 2, pp. 69-150, 1944.
- [51] W.J. Sette, "A new reverberation time formula," *J. Acoustical Soc.*, vol. 4, pp. 193-210, 1933.
- [52] G. Millington, "A modified formula for reverberation," *J. Acoustical Soc.*, vol. 4, pp. 69-82, 1932.
- [53] L.K Kinsler and A.R. Frey, *Fundamentals of Acoustics, second edition*. New York: John Wiley & Sons, 1962, chapter 14.
- [54] H. Kuttruff, *Room acoustics*. Norfolk, England: Applied Science Publishers LTD, 1973, chapter 5.
- [55] A. D. Pierce, *Acoustics: An Introduction to its Physical Principles and Applications*. Woodbury, NY: Acoustical Society of America, 1989, chapter 6.
- [56] K.K. Dunens and R.F. Lambert, "Impulsive sound-level response statistics in a reverberant enclosure," *J. Acoust. Soc. Am.*, vol. 61, no. 6, pp. 1524-1532, 1977.

- [57] E.T. Paris, "On the coefficient of sound-absorption measured by the reverberation method," *Phil. Mag.*, s. 7, vol. 5, no. 29, pp. 489-487, 1928.
- [58] T.F.W. Embleton, "Absorption coefficients of surfaces calculated from decaying sound fields," *Acoustical Soc. America*, vol. 50, no. 3, part 2, pp. 801-811, 1970.
- [59] D.A. Hill, "Electronic mode stirring for reverberation chambers," *IEEE Trans. Electromag. Compat.*, vol. 36, no. 4, pp. 294-299, 1994.
- [60] RH. Liu, D.C. Chang, and M.T. Ma, "Eigenmodes and the composite figure of merit of a reverberating chambers," *Nat. Bureau of Stand. Tech. Note 1066*, August, 1983.
- [61] M.T. Ma "Understanding reverberating chambers as an alternative facility for EMC testing," *J. Electromag. Wave Appl.*, vol. 2, nos. 3/4, pp. 339-351, 1988.
- [62] J.M. Dunn, "Local high-frequency analysis of the fields in a mode-stirred chamber," *IEEE Trans. Electromag. Compat.*, vol. 32, no. 1, pp. 53-58, 1990.
- [63] D.A. Hill, J.W. Adams, M.T. Ma, A.R. Ondrejka, M.L. Crawford, and R.T. Johnk, "Aperture excitation of electrically large, lossy cavities," *Nat. Inst. Stand. Tech. Technical Note 1361*, Sept. 1993.
- [64] J.M. Ladbury, R.T. Johnk, and A.R. Ondrejka, "Rapid evaluation of mode-stirred chambers using impulsive waveforms," *Nat. Inst. Stand. Tech. Technical Note 1381*, Jun. 1996.
- [65] D.A. Hill, "A reflection coefficient derivation for the Q of a reverberation chamber," *IEEE Trans. Electromag. Compat.*) vol. 38, no. 4, pp. 591-592, 1996.
- [66] C.W. Kosten, "The mean free path in room acoustics," *Acustica*, vol. 10, pp. 245-250, 1960.
- [67] F. V. Hunt, "Remarks on the mean free path problem," *J. Acoustical Soc. of America*, vol 36, no. 3, pp. 556-564, 1964.
- [68] L. Batchelder, "Reciprocal of the mean free path," *J. Acoustical Soc. America*, vol. 36, no. 3, pp. 551-555, 1964.
- [69] R.R. DeLyser, C.L. Holloway, R.T. Jonhk, A.R. Ondrejka, and M. Kanda, "Figure of merit for low frequency anechoic chambers based on absorber reflection coefficients," *IEEE Trans. Electromag. Compat.*) vol. 38, no. 4, 576-584, 1996.
- [70] L.M. Brekhovskikh, *Waves in Layered Media*. New York: Academic Press, 1960, chapter 1.
- [71] C.A. Balanis, *Advanced Engineering Electromagnetics*. New York: John Wiley & Sons, 1989, chapter 5.

- [72] K.S. Yee, "Numerical solution of initial boundary value problem involving Maxwell's equations in isotropic media," *IEEE Trans. Antenna and Propag.*, vol. 14, pp. 302-307, 1966.
- [73] A. Taflove, *Computational Electrodynamics: The Finite-Difference Time-Domain Method*. Boston: Artech House, 1995.
- [74] A. Taflove and M.E. Brodwin, "Numerical solution of steady-state electromagnetic scattering problems using the time-dependant Maxwell's equation," *IEEE Trans. Microwave Theory Tech.*, vol. 23, no. 8, pp. 623-630, 1975.
- [75] G.M. Smith, *Numerical Solution of Partial Differential Equation: Finite Difference Method) 3rd Ed.* Oxford: Clarendon Press, 1985.
- [76] J.P. Berenger, "A perfectly matched layer for the absorption of electromagnetic waves," *J. Computational Phys.*, vol. 114, pp. 185-200, 1994.
- [77] R.H. Espeland, E.J. Violette, and K.C. Allen, "Millimeter wave wide-band diagnostic probe measurements at 30.3 GHz on an 11.8 km link," NTIA Technical Memorandum 83-95, U.S. Department of Commerce, Boulder, CO., Sept. 1983.
- [78] P.B. Papazian, Y. Lo, E.E. Pol, M.P. Roadifer, T.G. Hoople, R.J. Achatz, "Wideband propagation measurements for wireless indoor communication," NTIA Report 93-292, NTIA/ITS, U.S. Department of Commerce, Boulder, CO., Jan. 1993.
- [79] W.B. Westphal and A. Sils, "Dielectric constant and loss data," *Technical Report AFML-TR-72-39*, Massachusetts Institute of Technology, Apr. 1972.
- [80] K. Sato, H. Kozima, H. Masuzawa, T. Manabe, T. Ihara, Y. Kassashima, and K. Yamaki, "Measurements of reflection characteristics and refractive indices of interior construction material in millimeter-wave bands," 1995 *IEEE 45th Vehicular Technology Conference*, Chicago, IL, 1995, pp. 449-453.
- [81] C.L. Holloway, P.L. Perini, R.R. DeLyser, and K.C. Allen, "Analysis of composite walls and their effects on short-path propagation modeling," *IEEE Trans. Veh. Technol.*, vol. 46, no. 3, pp. 730-738, 1997.
- [82] M.a. Al-Nuaimi and M.S. Ding, "Prediction models and measurements of microwave signals scattered from building," *IEEE Trans. Antenna Propagat.*, vol. 42, no. 8, pp. 1126-1137, 1994.
- [83] W. Honcharenko and H.L. Bertoni, "Transmission and reflection characterization of concrete block walls in the UHF bands proposed for future PCS," *IEEE Trans. Antennas Propag.*, vol. 43, no. 2, pp. 232-239, 1994.
- [84] O. Landron, M.L. Feuerstein, and T.S. Rappaport, "A comparison of theoretical and empirical reflection coefficients for typical exterior wall surfaces in a mobile radio environment," *IEEE Trans. Antennas Propag.*, vol. 44, no. 3, pp. 341-351, 1996.

BIBLIOGRAPHIC DATA SHEET

| | | | |
|--|--------------------|---|-------------------------------|
| | 1. PUBLICATION NO. | 2. Gov't Accession No. | 3. Recipient's Accession No. |
| 4. TITLE AND SUBTITLE A Simplified Model for Predicting the Power Delay Profile Characteristics of an Indoor Radio Propagation Channel | | 5. Publication Date | |
| | | 6. Performing Organization Code NTIA/ITS | |
| 7. AUTHOR(S) Christopher L. Holloway, Michael G. Cotton, Paul McKenna | | 9. Project/Task/Work Unit No. 8 910 8105 | |
| 8. PERFORMING ORGANIZATION NAME AND ADDRESS NTIA/ITS 325 Broadway Boulder, CO 80303-3328 | | 10. Contract/Grant No. | |
| 11. Sponsoring Organization Name and Address NTIA 1401 Constitution Ave, NW Washington, DC 20230 | | 12. Type of Report and Period Covered | |
| | | 13. | |
| 14. SUPPLEMENTARY NOTES | | | |
| 15. ABSTRACT (A 200-word or less factual summary of most significant information. If document includes a significant bibliography or literature survey, mention it here.) Multipath channels in indoor wireless communication systems exhibit a characteristic power delay profile, which can be a detriment to system performance. In this paper, we present a simplified model for calculating the decay rate of the power delay profile for propagation within rooms. This simplified model provides a time-efficient means of predicting system performance. Predictions of this indoor power delay profile (IPDP) model are compared to results obtained from a finite-difference time-domain (FDTD) model. Additionally, comparisons of the IPDP model to measured data are presented. The rms delay spread is the second central moment of the power delay profile of a propagation channel and is a measure of the communication link degradation due to multipath. We also show results of the estimated rms delay spread from this model and show comparisons to the measured data. This IPDP model can be used to investigate the effects of variable room size and properties of the surfaces (or walls) on the decay characteristics of the power delay profile. | | | |
| 16. Key Words (Alphabetical order, separated by semicolons) channel modeling; delay spread; finite-difference time-domain modeling; impulse response; multipath; power delay profile; | | | |
| 17. AVAILABILITY STATEMENT <input checked="" type="checkbox"/> UNLIMITED. <input type="checkbox"/> FOR OFFICIAL DISTRIBUTION. | | 18. Security Class. (This report) | 20. Number of pages 27 |
| | | 19. Security Class. (This page) | 21. Price: |